



# Experimental study on failure mechanism and geometric parameters of blasting crater under uniaxial static compressive stresses

Guangliang Yan<sup>1,2</sup> · Fengpeng Zhang<sup>1</sup> · Taeseo Ku<sup>2</sup> · Qiqi Hao<sup>1</sup>

Received: 30 April 2021 / Accepted: 18 April 2022 / Published online: 1 June 2022  
© Springer-Verlag GmbH Germany, part of Springer Nature 2022

## Abstract

In deep mining and rock engineering, it is important to understand the failure mechanism of a blasting crater under coupled dynamic and static loads, and further investigate the quantitative relationships between its parameters and the static stress. In this study, lab-scale crater-blasting experiments on sandstone specimens under different uniaxial stresses are performed to investigate the characteristics of the blasting craters and the blasting fragments as well as their representative failure mechanisms. The relationships between the diameter, area, volume of a blasting crater, and the stress–strength ratio (SSR) are analyzed quantitatively. The results show that the blasting crater can be divided into block, transition, and flaky failure zones. Correspondingly, the blasting fragments can be classified into block, transition, and flaky fragments. The block failure zone and the block fragments are caused by tensile and high-temperature burn damage. The transition failure zone and the transition fragments are the results of tensile and shear damage. The flaky failure zone and the flaky fragments are produced mainly by tensile damage. The relationships between the blasting crater parameters and the SSR can be divided into three stages: linear growth stage, slow growth stage, and rapid growth stage. The static stress has a significant influence on the blasting craters parallel to it, whereas it has a negligible effect on those perpendicular to it. Besides, the static stress leads to oversized fragments and has the most significant influence on the flaky failure zone. Finally, a blasting design method considering static stresses is proposed.

**Keywords** Static compressive stresses · Blasting crater · Blasting fragment · Failure mechanism · Blasting design method

## Introduction

In geomaterials and rocks, in situ stress gradually increases with the increase in depth (Kang et al. 2010; Heidebach et al. 2010). Generally, there is an approximate linear relationship between the in situ stress and depth (Li et al. 2019; Ku et al. 2017). The drilling-blasting method is still commonly used in deep rock engineering, such as for constructing mines, tunnels, and underground chambers. Specifically, in deep rock engineering, an intact rock is often degraded/broken under the coupling of dynamic and static loads. Numerous

studies have verified that the in situ stress has a dual influence on the blasting effect. The negative effect is that it can cause over- or under-excavation, produce oversized fragments, and even induce rock bursts (Zhang et al. 2020b; Niu et al. 2021), posing a major threat to lives, facilities, and production. Cai et al. (2020, 2021) explained the mechanism of rock burst based on the hypothesis of coupled static and dynamic stresses. On the positive side, the elastic energy stored in a high in situ stress rock mass is released by blasting, which, in turn, promotes the blasting effect (Xiao et al. 2019; Li et al. 2018). Therefore, understanding the failure mechanism of rocks under the coupling of dynamic and static loads and establishing a blasting design method considering in situ stresses are the basis and prerequisites for deep rock engineering.

The current studies have provided an insight into the influence of static stresses on the dynamic mechanical properties (Li et al. 2013, 2017) and failure behavior of rocks (Yao et al. 2019). Furthermore, static stress has a remarkable influence on crack formation and propagation (Hao et al.

✉ Fengpeng Zhang  
zhangfengpeng@mail.neu.edu.cn

<sup>1</sup> Key Laboratory of Ministry of Education On Safe Mining of Deep Metal Mines, Northeastern University, Shenyang 110819, China

<sup>2</sup> Department of Civil and Environmental Engineering, Konkuk University, Seoul 05029, Republic of Korea

2020; Yang and Ding 2018). Li et al. (2020a) performed model experiments and found that high static stress controls the fracture and failure pattern of a specimen. Under static stress, the formation and propagation of cracks parallel to the applied stress occur preferentially, whereas those perpendicular to it are inhibited (Yang et al. 2019; Li et al. 2020b). The static stress also changes the crack initiation mode. Under a biaxial static stress, radial cracks are inhibited to different degrees, whereas circumferential cracks are promoted during crater blasting (Zhang et al. 2020a).

The static stress of a rock affects the formation and propagation of cracks and subsequently impacts the shape of the blasting crater and the characteristics of the blasting fragments. Zhang et al. (2020a) found that under uniaxial and biaxial static stresses, a rock is more susceptible to flaky damage during blasting. However, they did not study the failure mechanism of the blasting fragments under these static stresses. The characteristics of blasting fragments under different static stresses and the influence of static stress on the blasting fragments have been rarely studied. Furthermore, the failure mechanisms of blasting fragments under coupled dynamic and static loads have not been explicitly determined.

Static stress affects not only the characteristics of blasting fragments but also the shape and size of the corresponding blasting failure zone. Anisotropic static stress fields produce an anisotropic failure zone (Zhang et al. 2017; Yilmaz and Unlu 2013). Similar to the influence of static stress on cracks, the blasting failure zone is preferentially developed in the direction of the static stress (Li et al. 2016b; Yi et al. 2018). However, the quantitative relationships between the diameter, area, volume, and other parameters of the blasting failure zone and the static stress are still unclear. Despite the abovementioned previous efforts, the design methods of shallow-blasting engineering are still widely adopted in deep rock engineering, and blasting design methods considering in situ stresses are lacking. In practice, the above problems have limited the development of deep rock engineering due to the lack of a reliable design methodology. Therefore, it is particularly important to study the quantitative relationships

between the static stress and the parameters of the blasting failure zone and to establish a blasting design method suitable for deep high-stress rock engineering.

The Livingston crater blasting theory (Fourney et al. 1991; Li et al. 2016a; Zhang et al. 2018) is commonly adopted as the theoretical basis of engineering blasting design. Therefore, in view of the above problems, in this study, a series of crater blasting experiments are conducted on green sandstone specimens under various uniaxial compressive stresses. The characteristics and the failure mechanisms of the blasting fragments and the blasting craters under static stresses are studied. The relationships between the blasting crater parameters and the static stress are analyzed quantitatively. Finally, based on these quantitative relationships, a blasting design method considering static stresses suitable for deep rock engineering is proposed.

## Experimental programs

### Experimental apparatus

The experimental apparatus (Peng et al. 2019) used in this study consisted of an electric explosion system, a biaxial loading system, and a control system, as shown in Fig. 1. The electric explosion system produced a metal wire electric explosion to simulate an explosion and impose an explosive dynamic load on a rock. The loading system was a biaxial loading press, which can impose different static stress fields on specimens to simulate the in situ stress state of a deep rock mass. The control system was a DG535 time-delay synchronization controller, whose function was to control the operation of the electric explosion system. Table 1 lists the main technical parameters of the experimental apparatus.

### Electrode and specimen

Figure 2 shows a schematic and photograph of the electrode. The electrode diameter was 10 mm, and the insulating rod material was polylactic acid, which was produced

**Fig. 1** Photos of experimental apparatus

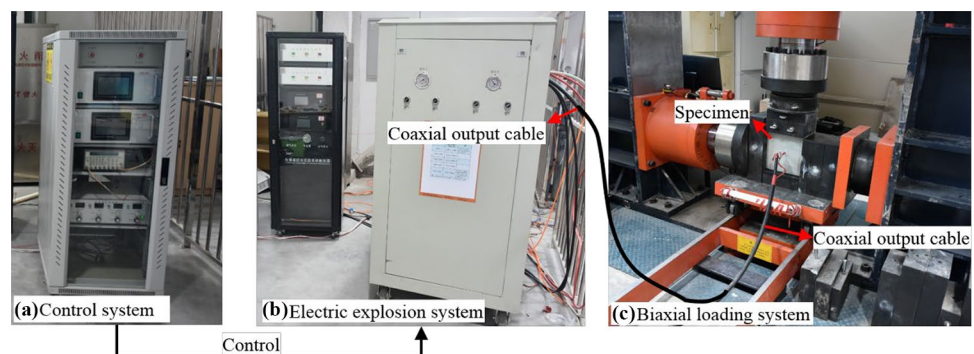


**Table 1** Main technical parameters of experimental apparatus

Subsystem	Technical index	Technical parameter
Electric explosion system	Rated voltage	± 30 kV
	Rated energy	7.2 kJ
Biaxial loading system	Maximum specimen size	500 × 500 × 250 mm <sup>3</sup>
	Horizontal and vertical maximum load	5000 kN
Control system	Precision	5 ps
	Time range	1 ns ~ 999 s

by three-dimensional (3D) printing. Two copper bars, each with a cross-sectional size of 2 mm × 4 mm, were connected to a copper wire at one end and the electric explosion system at the other end. The copper wire, 0.4 mm in diameter and 50 mm in length, was coiled into a symmetrical disc, as shown in Fig. 2.

The quasi-static mechanical parameters of the green sandstone used in these experiments are listed in Table 2. As shown in Fig. 3, these rock blocks were cut into cuboidal specimens with dimensions of 300 mm × 300 mm × 150 mm. The blasthole diameter, depth, and minimum resistance line were 12 mm, 130 mm, and 20 mm, respectively. The prepared electrode was inserted into the bottom of the blasthole and sealed with a quick-setting cement. After the quick-setting cement completely dried, crater-blasting experiments were conducted. In this study, the free surface of a specimen is defined as the *xy* plane; the origin, *o*, is the intersection of the center of the blasthole and the free surface; and the *z*-axis direction is perpendicular to the free surface, as shown in Fig. 3.

**Experimental scheme**

The crater-blasting experiments conducted in this study were divided into six groups of uniaxial static compressive stresses of 0, 8, 12, 16, 24, and 32 MPa, respectively, and

corresponding stress–strength ratios (SSRs) of 0, 0.1, 0.15, 0.2, 0.3, and 0.4.

The experimental procedure is outlined as follows.

- (1) The charging voltage of the electric explosion system and other equipment parameters were set such that all equipments were in standby states. In this study, the charging voltage was 50 kV and the energy storage was 5.0 kJ.
- (2) A specimen was placed in the biaxial loading system and connected to the electric explosion system.
- (3) A force-controlled loading method was used to apply a restraint load of 5 kN (0.11 MPa) on the specimen in the horizontal direction (*x*-axis direction) to prevent the specimen from moving and reduce the boundary effect. Subsequently, the designed static stress was applied in the vertical direction (*y*-axis direction).
- (4) The electric explosion system was charged to the designed voltage.
- (5) The control system was used to start the electric explosion system and complete the experimental process.

**Experimental results and analysis**

**Characteristics of blasting crater**

Photographs of a blasting crater, under different static stress conditions, presenting its characteristics are shown in Fig. 4. When no static stress is applied, the blasting crater has a circular shape, as shown in Fig. 4a. However, when static stress is applied to the specimen, the shape of the blasting crater becomes elliptical, with the long axis parallel to the static stress, as shown in Fig. 4b–f. In addition, with the increase in the static stress, the long axis of the blasting crater gradually

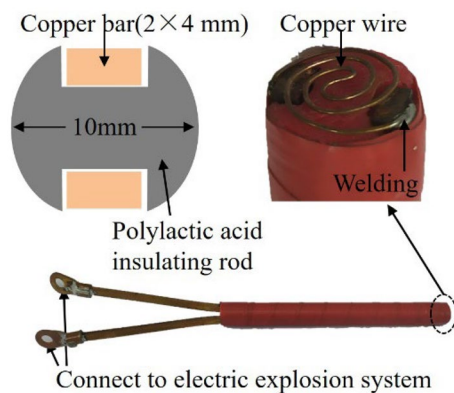


**Fig. 2** Schematic and photo of electrode

**Table 2** Sandstone mechanical parameters

Density kg/m <sup>3</sup>	Young’s modulus GPa	Poisson’s ratio	Wave velocity m/s	Compressive strength MPa	Tensile strength MPa
2472	27.9	0.22	5028	80.7	4.2

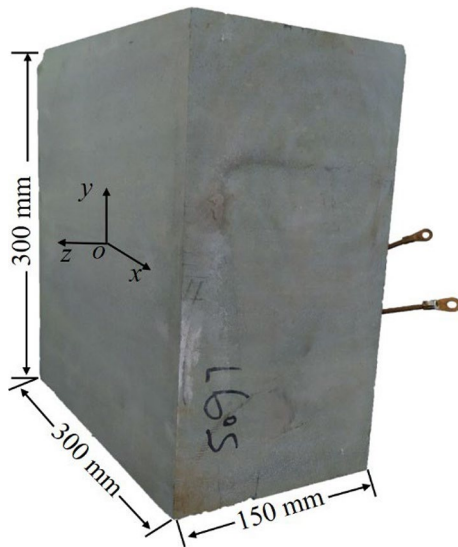


**Fig. 3** Photo of green sandstone specimen

increases. However, the static stress has little influence on the blasting crater in the direction perpendicular to it.

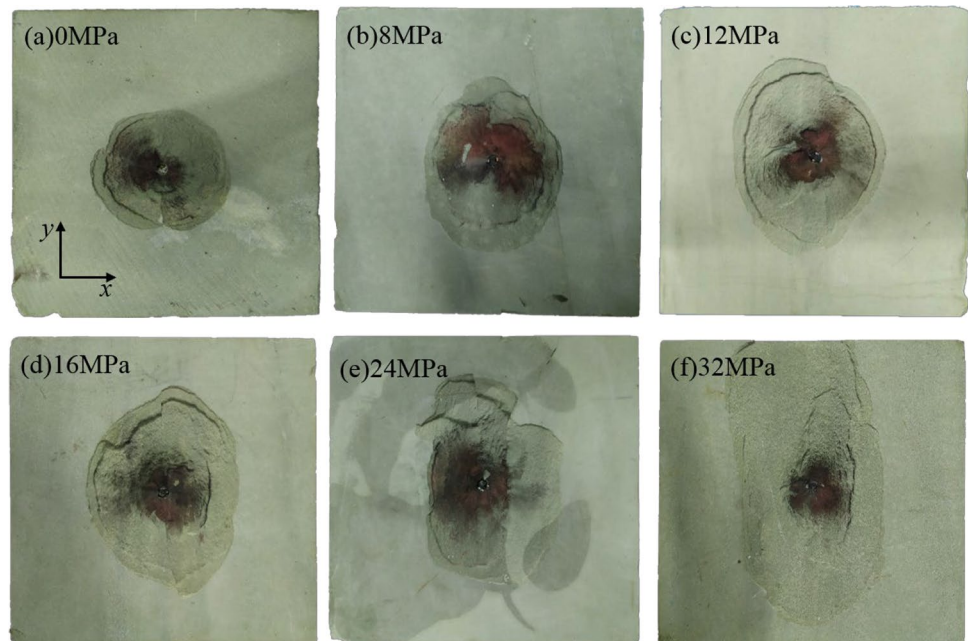
The block, transition, and flaky failure zones of a blasting crater without static stress are circular, as shown in Fig. 4a. When the SSR is 0.1 (see Fig. 4b), the block and transition failure zones are still circular and isotropic. However, the flaky failure zone is slightly elliptical, with the long axis parallel to the static stress direction. This indicates that when the SSR is 0.1, the static stress does not influence the block and transition failure zones, whereas it has a small effect on

the flaky failure zone. When the SSR values are 0.15 and 0.2, as shown in Fig. 4c and d, the block failure zone is still circular and isotropic. However, the transition failure zone becomes elliptical, with the long axis parallel to the static stress, and the elliptical shape of the flaky failure zone is comparatively clearer. When the SSR is 0.3, as shown in Fig. 4e, all three failure zones look elliptical, with the long axis parallel to the static stress. Similar to the SSR = 0.2 case, a clear crack parallel to the static stress is observable at the center of the blasting crater. When the SSR is 0.4, as shown in Fig. 4f, all three failure zones of the blasting crater remain elliptical, with the long axis parallel to the static stress. In addition, the elliptical shape is clearer in each failure zone compared to those at other SSRs.

The results in Fig. 4 show that the static stress first affects the flaky failure zone. When the static stress reaches a certain level, it affects the transition failure zone and subsequently the block failure zone. The static stress has the greatest influence on the flaky failure zone, followed by the transition and block failure zones.

To study the morphological characteristics of a blasting crater under static stress, a 3D scanner was used to scan and analyze its morphology. Figure 5 shows the morphological characteristics of a blasting crater at an SSR of 0.4, based on which the blasting crater is divided into three failure zones: block, transition, and flaky failure zones. In Fig. 5a, “Zone1” is the block failure zone, which is around the blasthole. From the cross-sectional views of the blasting crater, as shown in Fig. 5b and c, the blasting crater angle (Zhang et al. 2018) in the block failure zone is the largest. Not only that, the block failure zone has the largest depth and the blasting fragments

**Fig. 4** Blasting crater under different SSRs. **a, b, c, d, e, f** SSRs are 0, 0.1, 0.15, 0.2, 0.3, and 0.4, respectively



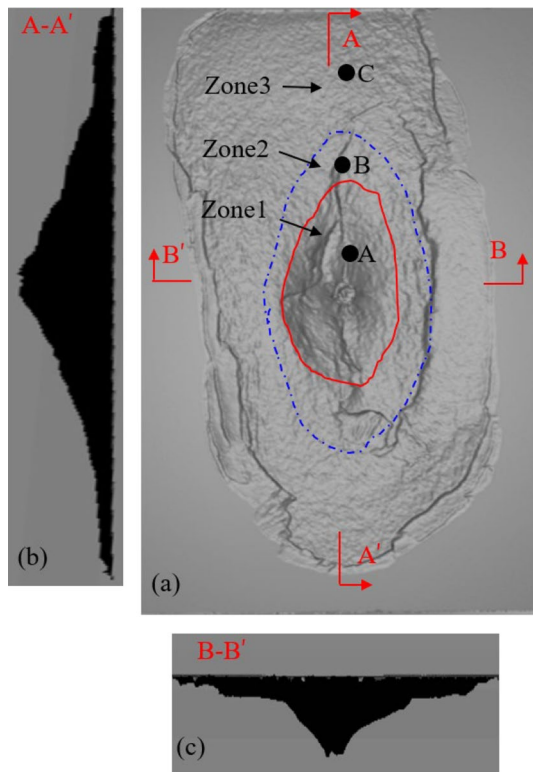


**Fig. 5** Scanning image of blasting crater under SSR of 0.4. **a** Blasting crater. **b** Cross-sectional view parallel to static stress. **c** Cross-sectional view perpendicular to static stress

in this zone are cubic. “Zone2” is the transition failure zone, which is between the block and flaky failure zones. In the direction parallel to the static stress, the blasting crater angle of the transition failure zone decreases as the distance from the blasthole increases (see Fig. 5b). However, in the direction perpendicular to the static stress, the blasting crater angle suddenly decreases (see Fig. 5c). Clearly, the transition failure zone parallel to the static stress is larger than that perpendicular to the static stress. In other words, in the direction parallel to the static stress, the block failure zone transits slowly to the flaky failure zone, but in the direction perpendicular to the static stress, the block failure zone transits rapidly to the flaky failure zone. Besides, the blasting fragments in the transition failure zone present a gradual transition from block failure to flaky failure. “Zone3” is the flaky failure zone, which is between the transition failure zone and the blasting crater boundary. The blasting crater angle in the flaky failure zone is the smallest, and its depth is also the smallest. The blasting fragments in the flaky failure zone are nearly two-dimensional (2D) flakes. Similar to the transition failure zone, the area of the flaky failure zone parallel to the static stress is more larger than that perpendicular to the static stress.

As shown in Fig. 5b, the blasting crater angle of the block failure zone, in the direction parallel to the static stress is large, and it slowly transitions from the block failure zone to the flaky failure zone, with a larger transition failure zone. In the direction perpendicular to the static stress, as shown in Fig. 5c, the blasting crater angle of the block failure zone is small, and it rapidly transitions from the block failure zone to the flaky failure zone, with a small transition failure zone.

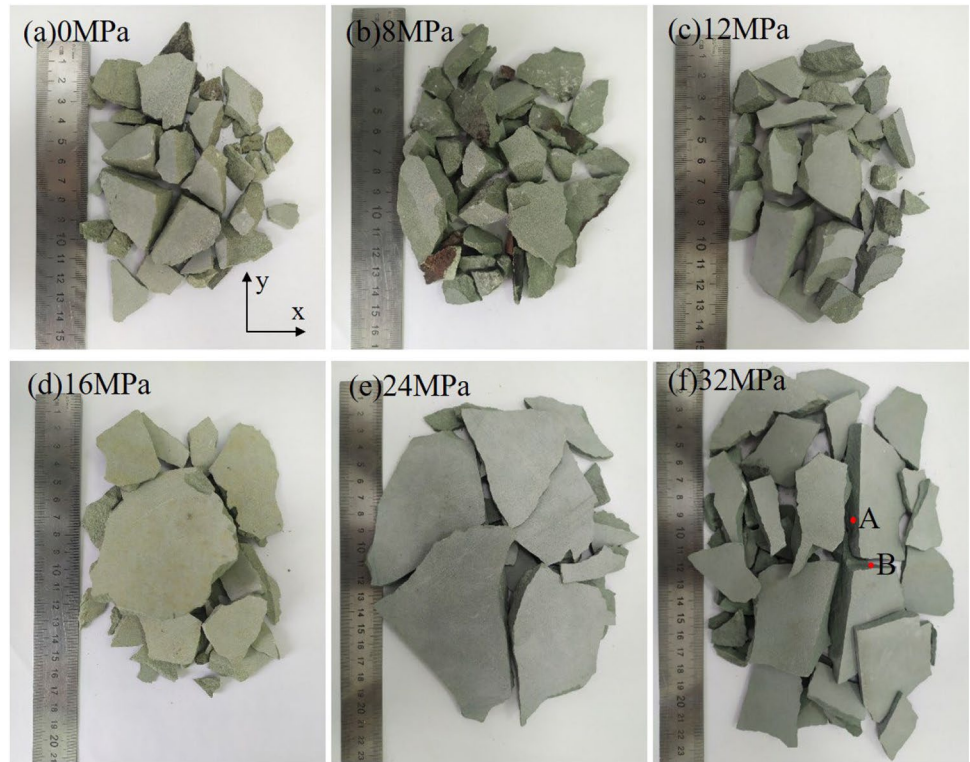
### Characteristics of blasting fragments

Static stress not only affects the shape of a blasting crater but also has a significant influence on the corresponding blasting fragments. Figure 6 shows the blasting fragments under different SSRs. Based on their morphological characteristics and corresponding to the failure zones of the blasting crater, the blasting fragments are classified into three types: block, transition, and flaky failure fragments. Interestingly, it is observed that the block failure fragments are cubic while the flaky failure fragments are 2D flakes. The transition failure fragments have the characteristics of both block and flaky failure fragments, and they are 3D at one end and similar to 2D flakes at the other end.

When the SSR is 0 (Fig. 6a), the blasting fragments mainly comprise block failure fragments and some flaky failure fragments. The fragment sizes are uniformly distributed, and no clear oversized fragments are produced. When the SSR is 0.1 (Fig. 6b), the blasting fragments are still mainly from the block failure fragments, and the fragment sizes are basically the same as those when the SSR is 0, which indicates that when the SSR is small, static stress does not have a significant influence on the blasting fragments. When the SSR is 0.15 (Fig. 6c), the blasting fragment characteristics are different from those when the SSRs are 0 and 0.1. In this case, although the blasting fragments still consist of mainly block failure fragments and few flaky failure fragments, the former are elongated. This is because the static stress promotes crack propagation parallel to its direction but inhibits that perpendicular to its direction (Yang and Ding 2018; Yang et al. 2019; Zhang et al. 2020a). Therefore, the long axis of a block failure fragment is parallel to the static stress direction. The above results show that when the SSR is 0.15 and above, the influence of the static stress on the blasting fragments needs to be considered in the blasting design.

When the SSR is 0.2 (Fig. 6d), an oversized fragment is formed at the center of the blasthole, and the blasting fragment sizes are no longer uniform. When the SSRs are 0.3 and 0.4 (Fig. 6e and f), both blasting fragment masses and sizes are significantly greater than under the smaller static stress condition. Simultaneously, there is a greater increase in the flaky failure fragments than those in the other fragments.

**Fig. 6** Blasting fragments under different SSRs. **a, b, c, d, e, f** SSRs are 0, 0.1, 0.15, 0.2, 0.3, and 0.4, respectively



Based on the above results, the static stress produces oversized fragments and increases the number of blasting fragments, particularly the flaky fragments. However, Figs. 4 and 6 show that the static stress increases only the blasting fragments parallel to its own direction, whereas it has little influence on the blasting crater in the direction perpendicular to the applied stress.

**Parameters of blasting crater**

The diameter, area, and volume of a blasting crater are measured to investigate the quantitative relationships between the blasting crater parameters and the static stress. Simultaneously, the blasting crater parameters are made dimensionless to quantitatively analyze the influence of the static stress. The diameter increment ratio, area increment ratio and volume increment ratio are introduced.

$$\begin{aligned} \alpha_{xi} &= \frac{D_{xi} - D_{x0}}{D_{x0}} \times 100\% \\ \alpha_{yi} &= \frac{D_{yi} - D_{y0}}{D_{y0}} \times 100\% \end{aligned} \tag{1}$$

where  $\alpha_{xi}$  and  $\alpha_{yi}$  are the increments in the blasting crater diameters perpendicular and parallel to the static stress at the SSR =  $i$ , respectively;  $D_{xi}$  and  $D_{yi}$  are the blasting crater diameters perpendicular and parallel to the static stress direction at the SSR =  $i$ , respectively;  $D_{x0}$  and  $D_{y0}$  are the blasting crater diameters in the absence of the static stress. In this study,  $i = 0.1, 0.15, 0.2, 0.3, \text{ and } 0.4$ .

$$\beta_i = \frac{A_i - A_0}{A_0} \times 100\% \tag{2}$$

where  $\beta_i$  is the increment in the blasting crater area at the SSR =  $i$ ,  $A_i$  is the blasting crater area at the SSR =  $i$ , and  $A_0$  is the blasting crater area in the absence of static stress.

$$\gamma_i = \frac{V_i - V_0}{V_0} \times 100\% \tag{3}$$

where  $\gamma_i$  is the increment in the blasting crater volume at the SSR =  $i$ ,  $V_i$  is the blasting crater volume at the SSR =  $i$ , and  $V_0$  is the blasting crater volume in the absence of static stress.

**Diameter of blasting crater**

The quantitative relationship between the blasting crater diameter and the SSR and the influence of the static stress on the former are analyzed. The increments in the blasting crater diameter under different SSRs are calculated using Eq. (1). Figure 7 shows the quantitative relationships among the blasting crater diameters ( $D_{xi}$  and  $D_{yi}$ ), increments in the diameters, and SSR. It can be seen that the variation in the diameter perpendicular to the static stress,  $D_{xi}$ , is small, and its maximum increment does not exceed 20%. Therefore, the influence of the static stress on the blasting crater diameter perpendicular to it is almost negligible.

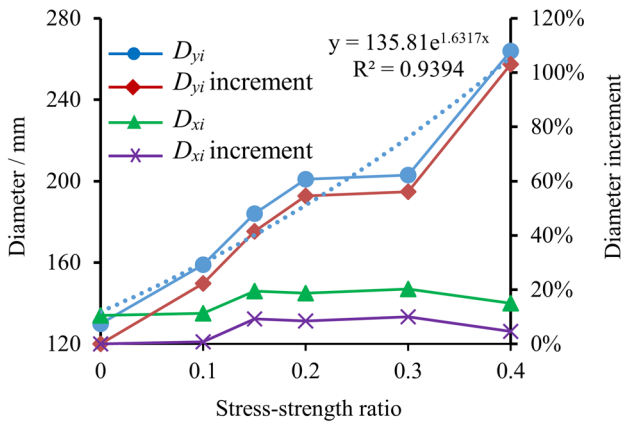


Fig. 7 Blasting crater diameters and diameter increments under different SSRs

However, the diameter parallel to the static stress,  $D_{yi}$ , gradually increases with the increase in the SSR. When the SSR is 0.1, the static stress has a significant influence on  $D_{yi}$ , with an increment of 22%. When the SSR increases from 0.2 to 0.3, the increment in  $D_{yi}$  is only 1%, indicating that  $D_{yi}$  presents a gradual growth phase. When the SSR reaches 0.4,  $D_{yi}$  increases rapidly up to 103%.

**Area of blasting crater**

To study the quantitative relationship between the blasting crater area and the SSR and the influence of the static stress on the former, an Artec Space Spider 3D scanner is used to measure the blasting crater area. The increments in the blasting crater area under different SSRs are calculated using Eq. (2).

The quantitative relationships among the blasting crater area, area increment, and SSR are presented in Fig. 8.

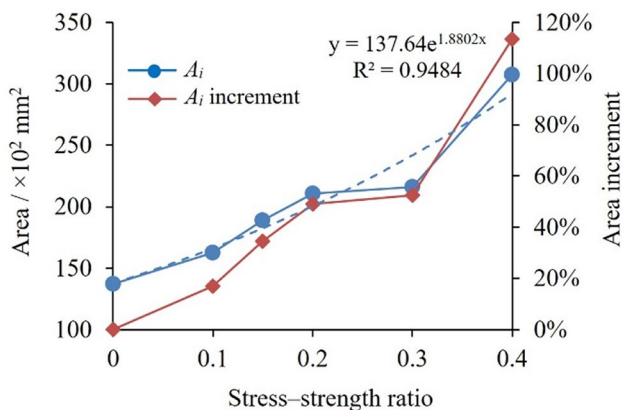


Fig. 8 Blasting crater areas and area increments under different SSRs

As the SSR gradually increases, the blasting crater area also gradually increases. When the SSR is 0.1, the increment in the blasting crater area is 17%. When the SSR increases to 0.2, the increment in the blasting crater area increases to 49%. When the SSR increases from 0.2 to 0.3, the increment in the blasting crater area is insignificant, only 4%. When the SSR reaches 0.4, the blasting crater area increases rapidly, with an increment of 114%.

**Volume of blasting crater**

This section presents the analysis of the quantitative relationship between the blasting crater volume and the SSR as well as the influence of the static stress on the relationship. The increments in the blasting crater volume under different SSRs are calculated using Eq. (3).

Figure 9 shows the quantitative relationships between the blasting crater volume, volume increment, and SSR. It can be seen that as the SSR gradually increases, the blasting crater volume also gradually increases. When the SSR is 0.1, the volume increment is 10%, which is very small under this condition. When the SSR is 0.15, the volume increment is 18%, and the influence of the static stress on the blasting crater volume is non-negligible. Specifically, when the SSR is 0.15 and above, the influence of the static stress on the blasting volume needs to be considered in blasting design. When the SSR increases to 0.2, the blasting crater volume continues to increase. However, when the SSR increases from 0.2 to 0.3, the increment in the blasting crater volume is only 4%. This indicates that the influence of the static stress on the blasting crater volume is not significant, presenting a stabilization phase. When the SSR is 0.4, the blasting crater volume increment reaches 71%.

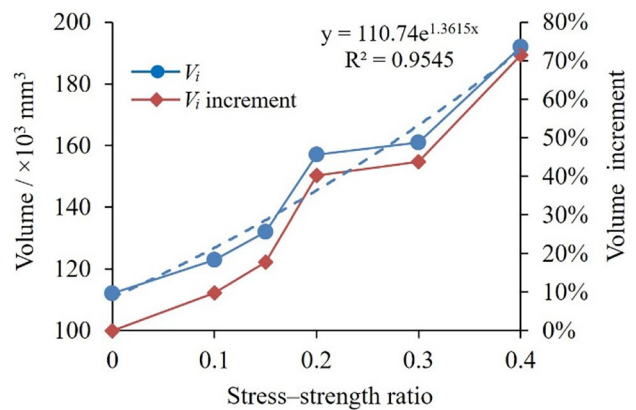
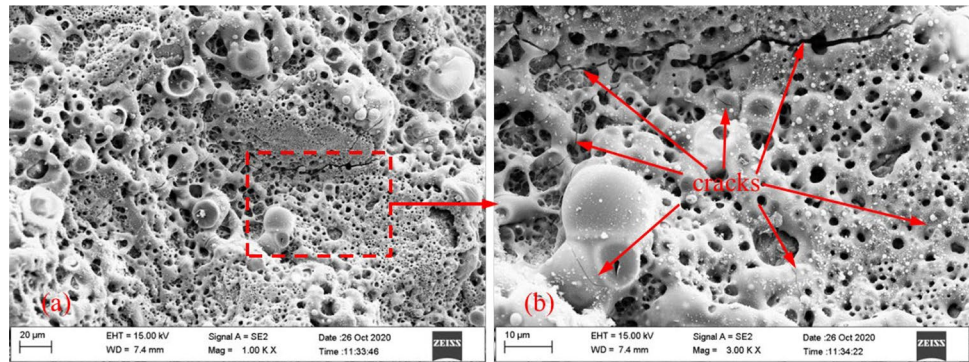


Fig. 9 Blasting crater volumes and volume increments under different SSRs

**Fig. 10** SEM fractography images of block failure zone. **a** Magnification 1000 $\times$ . **b** Magnification 3000 $\times$



## Discussion

### Failure mechanism of blasting crater

Scanning electron microscopy (SEM) is an effective method for studying the failure mechanism of rocks (Xu et al. 2019; Zhao et al. 2018). To study the failure mechanism of the block, transition, and flaky failure zones, samples were examined at points A, B, and C, respectively, shown in Fig. 5, for the SEM analysis.

### Failure mechanism of block failure zone

The SEM microfractography images of the block failure zone at magnifications of 1000 $\times$  and 3000 $\times$ , presented in Fig. 10, show that it involves a high-temperature burning bubble-like area. The wire electric explosion is a high-temperature and high-pressure process, and the high temperature generated by the electric explosion results in the burning bubble-like block failure area.

Figure 10b shows a partially enlarged view of Fig. 10a. It can be seen that the rock is densely covered with snake-shaped microcracks of different widths and lengths. Under the action of the shock wave, the local stress concentration leads to the formation of microcracks. The microcracks are rapidly passivated to form holes, and the holes become

connected to each other to form penetration cracks. When adjacent cracks join, the rock undergoes brittle fracture (Zhao et al. 2018). Although the high temperature destroys the fracture morphology characteristics of the block failure zone caused by the shock wave, it can be speculated that the shock wave provoked by the wire electric explosion propagates in the direction of the free surface and causes tensile fracture of the rock. Therefore, the failure mechanism of the block failure zone is jointly affected by tensile and high-temperature burn damage.

### Failure mechanism of transition failure zone

Figure 11 shows the microfractography images of the transition failure zone at magnifications of 1000 $\times$  and 3000 $\times$ . Although the transition failure zone is also subjected to the high temperature of the wire electric explosion, the degree of burn is very small compared to the block failure zone, and the fracture characteristics are clearly visible.

In Fig. 11b, clear scratches are observed on the fracture surface and a lot of debris is distributed, which indicates that the transition failure zone is subjected to shear damage. Concurrently, the fracture surface is smooth, except for the shear damage zone in Fig. 11a, which indicates that the transition failure zone is also subjected to tensile damage. Moreover, the tensile damage zone accounts for a larger proportion of the transition failure zone than the shear damage zone. The

**Fig. 11** SEM fractography images of transition failure zone. **a** Magnification 1000 $\times$ . **b** Magnification 3000 $\times$

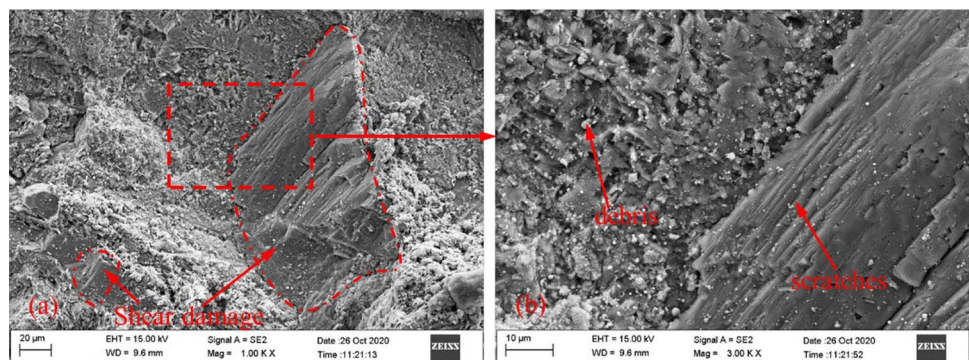
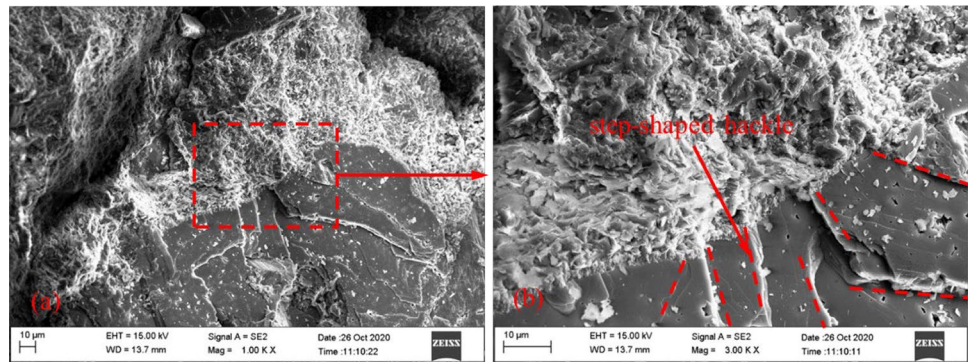




**Fig. 12** SEM fractography images of flaky failure zone. **a** Magnification 1000 $\times$ . **b** Magnification 3000 $\times$



above results show that the transition failure zone is caused by joint tensile and shear damage, where the tensile damage is dominant and the shear damage is supplementary.

### Failure mechanism of flaky failure zone

Figure 12 shows the microfractography images of the flaky failure zone at magnifications of 1000 $\times$  and 3000 $\times$ . It can be seen that the flaky failure zone is unaffected by the high temperature of the wire electric explosion. Concurrently, the fracture surface of the flaky failure zone is smooth and clean, without scratches and debris. In addition, fracture occurs on the crystal faces, which are parallel but not coplanar to each other. According to the fractography theory, a step-shaped hackle (Fig. 12b) constitutes a significant feature of brittle fracture (Feng et al. 2020). At a free surface, the shock wave is prone to reflection and transmission. Therefore, it can be speculated that the failure mechanism of the flaky failure zone is the tensile damage caused by the reflection and transmission actions of the shock wave.

### Failure mechanism of blasting fragment

#### Failure mechanism of block fragment

A block fragment contains three fracture surfaces: fracture surfaces adjoining the block failure zone, parallel to

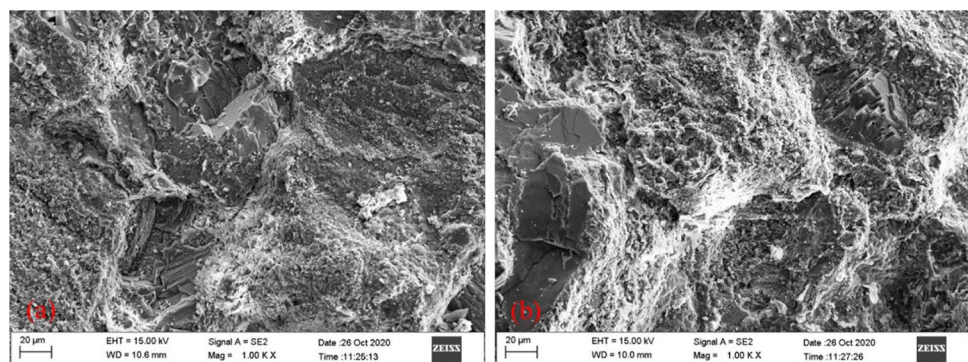
the static stress direction, and perpendicular to the static stress direction. The block failure zone is produced by high-temperature burn damage and shock wave tensile damage. Therefore, the adjoining fracture surface of a block fragment is also a result of both damages.

To study the fracture mechanisms of parallel and perpendicular static stress fracture surfaces, samples were examined at points A and B of a block fragment, as shown in Fig. 6f for the SEM analysis. Figure 13a and b shows the microfractography images of the fracture surfaces parallel and perpendicular to the static stress, respectively. In Fig. 13a, the fracture surface parallel to the static stress is characterized by intergranular fracture, and there are no scratches and debris on the surface, indicating that the fracture surface is caused by tensile damage. Interestingly, the fracture surface perpendicular to the static stress, as displayed in Fig. 13b, has the similar microscopic characteristics as that parallel to the static stress. Therefore, the perpendicular static stress fracture surface is also produced by tensile damage. In summary, the examined block fragment is produced by high-temperature burn damage and tensile damage, with the latter being dominant.

#### Failure mechanism of transition fragment

Although blasting fragments are classified into block, transition, and flaky fragments, the transition fragments are

**Fig. 13** SEM fractography of block failure fragment at magnification 1000 $\times$ . **a** Fracture surface parallel to static stress. **b** Fracture surface perpendicular to static stress



rare and mostly connected to block fragments. A transition fragment contains two fracture surfaces: fracture surfaces adjoining the transition failure zone (as shown in Fig. 11) and parallel to the static stress (as shown in Fig. 13a). Therefore, it can be determined that a transition fragment is generated by the shear and tensile damage.

### Failure mechanism of flaky fragment

A flaky fragment is a 2D flake, and its fracture surface is mainly the surface adjoining the flaky failure zone. The fracture surface of a flaky fragment can be considered to have the same characteristics as the flaky failure zone, as shown in Fig. 12. Therefore, the failure mechanism of a flaky fragment is the tensile damage, the same as that of the flaky failure zone.

### Effects of static stress on blasting crater parameters

As shown in Figs. 7, 8, and 9, the relationships between the blasting crater diameter parallel to the static stress, area, volume, and SSR present similar trends. Based on Figs. 7, 8, and 9, the blasting crater parameters increase obviously with the increase in the SSR when the SSR is between 0 and 0.2. However, when the SSR is between 0.2 and 0.3, the blasting crater parameters change slightly. Moreover, when the SSR exceeds 0.3, the blasting crater parameters increase sharply. The experimental results show that the relationship between each blasting crater parameter and the SSR can be divided into three phases: (1) a linear growth stage when the SSR is 0–0.2, (2) a gradual growth stage when the SSR is 0.2–0.3, and (3) a rapid growth stage when the SSR is 0.3–0.4.

Figure 14 shows the relationships between the increments in the blasting crater parameters and the SSR. Although

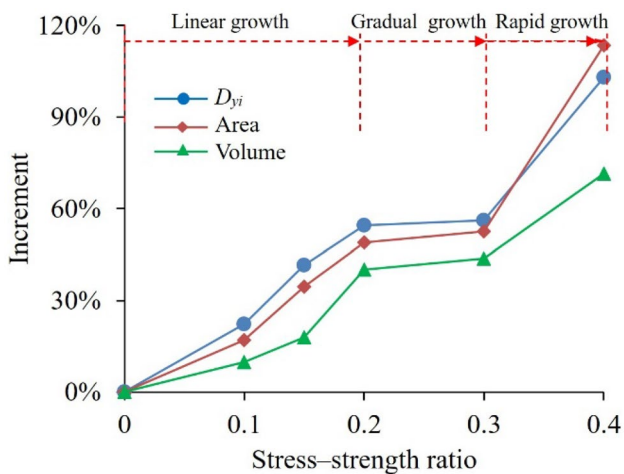


**Fig. 14** Relationships among increments in blasting crater parameters and SSR

the increments in the blasting crater diameter parallel to the static stress, area, and volume present similar trends, their magnitudes are rather different. At the same SSR, the increments in the blasting crater diameter and the blasting crater area are similar, but the increments in the blasting crater volume are smaller than them. Therefore, the influence of the static stress on the volume is less than that on the diameter and the area. This is because the static stress mainly increases the flaky failure zone, which is shallow and accounts for a smaller proportion of the blasting crater volume.

### Blasting design method considering static stress

Figure 4 shows that an anisotropic static stress field produces anisotropic blasting craters, indicating that the influence of static stress on the blasting crater shape needs to be considered in the blasting design. In Fig. 9, the blasting crater volume increases with the static stress, which means that the explosive unit consumption should be reduced. This is because a blasting disturbance induces the release of the elastic energy in a rock mass (Liu et al. 2017; Kuili and Sastry 2018; Xiao et al. 2019). However, Fig. 6 shows that static stress also leads to the formation and increase of oversized fragments, indicating that the explosive unit consumption should be increased. Therefore, it is necessary to comprehensively consider the effects of static stresses on the blasting crater shape, volume, and blasting fragment size in the blasting design.

Figure 15 shows a schematic of the coverage area of the blasthole in the absence and presence of static stress. In the absence of static stress, the blasting crater is circular (Fig. 4a). Therefore, the coverage area of the blasthole is also circular (Fig. 15a). However, under static stress, the blasting crater becomes elliptical, with the long axis parallel to the static stress, as presented in Fig. 4c–f. If the blasthole arrangement pattern without consideration of static stresses is still used, the adjacent blasthole coverage areas will considerably overlap in the static stress direction, as shown in Fig. 15b, which, in turn, will lead to problems

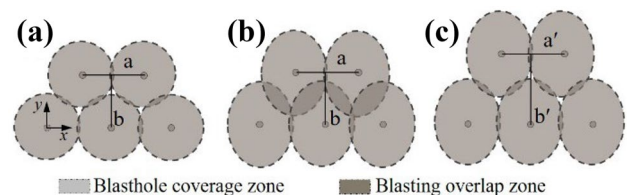


**Fig. 15** Schematic of blasthole coverage area. **a** without static stress. **b** without changing blasthole spacing under static stress. **c** with changing blasthole spacing under static stress

such as excessive damage and over-excavation. Therefore, it is necessary to adjust the blasthole spacing under static stress so that it uniformly covers the blasting area, as shown in Fig. 15c.

When only considering the influence of static stress on the blasting crater shape, the blasthole spacing should be modified as follows:

$$\begin{aligned} a'_i &= a \times (\alpha_{yi} + 1) \\ b'_i &= b \times (\alpha_{xi} + 1) \end{aligned} \tag{4}$$

where  $a$  and  $b$  are the blasthole spacings without static stress, and  $a'_i$  and  $b'_i$  are the blasthole spacings parallel and perpendicular to the static stress, respectively, as shown in Fig. 15.

In Eq. (4),  $\alpha_{xi}$  is approximately 0, and  $\alpha_{yi}$  increases gradually with the increase in the SSR. Therefore, with the increase in the static stress, the blasthole spacing perpendicular to it remains unchanged, whereas that parallel to the static stress gradually increases.

Figure 9 shows that the blasting crater volume gradually increases with the increase in the SSR. Therefore, the static stress also affects the explosive unit consumption. Explosive unit consumption is one of the main factors in the blasting design, which is defined as follows (Gasparyan 1979):

$$q = \frac{Q_e}{Q_r} \tag{5}$$

where  $q$  is the explosive unit consumption,  $\text{kg}/\text{m}^3$ ;  $Q_e$  is the amount consumption of explosives,  $\text{kg}$ ; and  $Q_r$  is the volume of rock broken by blasting,  $\text{m}^3$ .

When the SSR is varied, the explosive unit consumption can be modified as follows:

$$q_i = \frac{Q_e}{Q_r(1 + \gamma_i)} \tag{6}$$

As shown in Fig. 6c–f, the blasting fragment size clearly increases with the static stress. Therefore, when designing blasting, the influence of static stress on the blasting fragment size should also be considered. The fragment size can be reduced by two methods: (1) increasing the explosive unit consumption without changing the blasthole spacing, and (2) reducing the blasthole diameter and spacing and increasing the number of blastholes for more uniformly distributing the explosives.

Previous studies have shown that the drilling speeds of small-diameter drills are higher than those of large-diameter drills under the same conditions. For each 1-mm reduction in the bit diameter, the drilling speed is increased by 3–4% (He and Qian 2010). Small-diameter drill and small-diameter charge-blasting technology can improve excavation speed. Simultaneously, it results in uniform distribution of the

explosives, which helps in improving the blasting quality. Therefore, in this study, reducing the diameters and the spacings of blastholes and increasing the number of blastholes are suggested to control the blasting fragment size. When considering the influence of static stress on the blasting crater shape and blasting fragments size, the adjusted blasthole spacing with variation in the SSR can be expressed as follows:

$$\begin{aligned} a'_i &= a \times (\alpha_{yi} + 1) \times \lambda \\ b'_i &= b \times (\alpha_{xi} + 1) \times \lambda \end{aligned} \tag{7}$$

where  $\lambda$  is the blasthole diameter reduction coefficient.

$\lambda$  is defined as the ratio of the blasthole diameter under static stress to that under no static stress.

$$\lambda = R'/R \tag{8}$$

where  $R'$  is the reduced diameter of the blasthole under static stress and  $R$  is the original diameter of the blasthole under no static stress.

After the spacing and diameter of the blasthole are determined, the adjusted explosive unit consumption with the variation in the SSR can be obtained as follows:

$$q'_i = \frac{Q_e}{Q_r(1 + \gamma_i)} \times \eta_i \tag{9}$$

where  $\eta_i$  is the increase in the coefficient of explosive unit consumption under static stress.

$\eta_i$  is defined as the ratio of the explosive unit consumption at an SSR to that under no static stress at the same blasting fragment size.  $\eta_i$  can be determined based on actual site conditions. As static stress increases the blasting fragment size, the explosive unit consumption under the static stress must be increased to achieve a smaller blasting fragment size. Therefore, the increase in the coefficient of the explosive unit consumption,  $\eta_i$ , is greater than 1. After the determination of the blasthole diameter, blasthole spacing, and explosive unit consumption using Eqs. (7)–(9), other blasting parameters can be selected based on an existing blasting design method.

This blasting design method considers the influence of static stress on the blasting crater shape, volume, and blasting fragment size, which is beneficial for deep rock engineering. However, it should be noted that this blasting design method only considers the influence of a uniaxial static stress on blasting. A blasting design method considering biaxial stresses needs to be studied further. Moreover, this method needs to reduce the blast hole diameter and increase the number of blast hole, which means that the cost of drilling will increase. In addition, the blasting design method also lacks the validation of field experiments, and the factors of the influence of static stress on the blasting failure zone,

such as  $\alpha_{xi}$ ,  $\alpha_{yi}$ ,  $\beta_i$ ,  $\gamma_i$ , and  $\eta_i$ , need to be obtained by conducting numerous field experiments.

## Conclusions

In this study, crater-blasting experiments on sandstone specimens under various uniaxial compressive static stresses were performed. The following conclusions are drawn.

- (1) The blasting crater can be divided into block, transition, and flaky failure zones. Correspondingly, the blasting fragments can be classified into block, transition, and flaky fragments. The block failure zone and the block fragments are caused by tensile and high-temperature burn damage. The transition failure zone and the transition fragments are produced jointly by tensile and shear damage. The flaky failure zone and the flaky fragments are caused mainly by tensile damage.
- (2) When the SSR is 0.1, the uniaxial static stress has a significant influence on the diameter and area, whereas it has little influence on both volume of the blasting crater and fragment size. When the SSR is 0.15, the static stress has a significant influence on both blasting crater volume and fragment size. When the SSR is 0.2, it tends to generate oversized blasting fragments. When the SSR is 0.4, the blasting crater parameters sharply increase.
- (3) The influence of the uniaxial static stress on each blasting crater parameter can be divided into three stages: (1) linear growth stage when the SSR is between 0 and 0.2, (2) gradual growth stage when the SSR is between 0.2 and 0.3, and (3) rapid growth stage when the SSR is between 0.3 and 0.4.
- (4) The uniaxial static stress has a significant influence on the blasting craters parallel to it, whereas it has a negligible effect on those perpendicular to the applied stress. The static stress tends to produce oversized fragments and has the most influence on the flaky failure zone, followed by the transition and block failure zones.
- (5) A blasting design method considering the static stress that is applicable to deep rock engineering is proposed based on the quantitative relationships among the blasting crater parameters and the static stress.

**Acknowledgements** The authors would like to thank Mr. You Ji, Mr. Zhouhong Han, and Mr. Chuan Du for their kind assistance in experiments.

**Funding** The authors gratefully acknowledge the financial support from the State Key Research Development Program of China (Grant No. 2017YFC0602902). The first author wish to express his thanks to

China Scholarship Council (Grant No. 202006080082) for the financial support of his study.

## Declarations

**Conflict of interest** The authors declare no competing interests.

## References

- Cai W, Bai XX, Si GY, Cao WZ, Gong SY, Dou LM (2020) A monitoring investigation into rock burst mechanism based on the coupled theory of static and dynamic stresses. *Rock Mech Rock Eng* 53:5451–5471. <https://doi.org/10.1007/s00603-020-02237-6>
- Cai W, Dou LM, Si GY, Hu YW (2021) Fault-induced coal burst mechanism under mining-induced static and dynamic stresses. *Eng PRC* 7:687–700. <https://doi.org/10.1016/j.eng.2020.03.017>
- Feng JJ, Wang EY, Huang QS, Ding HC, Zhang XY (2020) Experimental and numerical study of failure behavior and mechanism of coal under dynamic compressive loads. *Int J Min Sci Technol* 30:613–621. <https://doi.org/10.1016/j.ijmst.2020.06.004>
- Fourney WL, Dick RD, Wang XJ, Wei Y (1991) Fragmentation mechanism in crater blasting. *Int J Rock Mech Min Sci* 30:413–429. [https://doi.org/10.1016/0148-9062\(93\)91723-V](https://doi.org/10.1016/0148-9062(93)91723-V)
- Gasparyan SA (1979) Effect of unit consumption of explosives on efficiency of tunnel heading advance. *Hydrotech Constr* 13:647–655. <https://doi.org/10.1007/BF02305195>
- Hao XJ, Du WS, Zhao YX, Sun ZW, Zhang Q, Wang SH, Qiao HQ (2020) Dynamic tensile behaviour and crack propagation of coal under coupled static-dynamic loading. *Int J Min Sci Technol* 30:659–668. <https://doi.org/10.1016/j.ijmst.2020.06.007>
- He MC, Qian QH (2010) The basis of deep rock mechanics. Science Press, Beijing (In Chinese)
- Heidbach O, Tingay M, Barth A, Reinecker J, Kurfess D, Muller B (2010) Global crustal stress pattern based on the world stress map database release 2008. *Tectonophysics* 482:3–15. <https://doi.org/10.1016/j.tecto.2009.07.023>
- Kang H, Zhang X, Si L, Wu Y, Gao F (2010) In-situ stress measurements and stress distribution characteristics in underground coal mines in China. *Eng Geol* 116:333–345. <https://doi.org/10.1016/j.enggeo.2010.09.015>
- Ku T, Subramanian S, Moon SW, Jung JW (2017) Stress dependency of shear wave velocity measurements in soils. *J Geotech Geoenviron Eng* 143:04016092. [https://doi.org/10.1061/\(ASCE\)GT.1943-5606.0001592](https://doi.org/10.1061/(ASCE)GT.1943-5606.0001592)
- Kuili S, Sastry VR (2018) A numerical modelling approach to assess the behaviour of underground cavern subjected to blast loads. *Int J Min Sci Technol* 28:975–983. <https://doi.org/10.1016/j.ijmst.2018.05.015>
- Li DY, Xiao P, Han ZY, Zhu QQ (2020a) Mechanical and failure properties of rocks with a cavity under coupled static and dynamic loads. *Eng Fract Mech* 225:106195. <https://doi.org/10.1016/j.engfracmech.2018.10.021>
- Li HB, Li JC, Liu B (2013) Direct tension test for rock material under different strain rates at quasi-static loads. *Rock Mech Rock Eng* 46:1247–1254. <https://doi.org/10.1007/s00603-013-0406-7>
- Li J, Wu CQ, Hao H, Wang ZQ, Su Y (2016a) Experimental investigation of ultra-high performance concrete slabs under contact explosions. *Int J Impact Eng* 93:62–75. <https://doi.org/10.1016/j.ijimpeng.2016.02.007>
- Li P, Cai MF, Guo QF, Miao SJ (2019) In situ stress state of the northwest region of the jiaodong peninsula, China from overcoring stress measurements in three gold mines. *Rock Mech Rock Eng* 52:4497–4507. <https://doi.org/10.1007/s00603-019-01827-3>

- Li XB, Gong FQ, Tao M, Dong LJ, Du K, Ma CD, Zhou ZL, Yin TB (2017) Failure mechanism and coupled static-dynamic loading theory in deep hard rock mining: a review. *J Rock Mech Geotech Eng* 9:767–782. <https://doi.org/10.1016/j.jrmge.2017.04.004>
- Li XB, Li CJ, Cao WZ, Tao M (2018) Dynamic stress concentration and energy evolution of deep-buried tunnels under blasting loads. *Int J Min Sci Technol* 104:131–146. <https://doi.org/10.1016/j.ijrmms.2018.02.018>
- Li XD, Liu KW, Yang JC, Nascimbene R (2020b) Study of the rock crack propagation induced by blasting with a decoupled charge under high in situ stress. *Adv Civ Eng* 2020:9490807. <https://doi.org/10.1155/2020/9490807>
- Li YH, Peng JY, Zhang FP, Qiu ZG (2016b) Cracking behavior and mechanism of sandstone containing a pre-cut hole under combined static and dynamic loading. *Eng Geol* 213:64–73. <https://doi.org/10.1016/j.enggeo.2016.08.006>
- Liu CY, Yang JX, Yu B (2017) Rock-breaking mechanism and experimental analysis of confined blasting of borehole surrounding rock. *Int J Rock Mech Min Sci* 27:795–801. <https://doi.org/10.1016/j.ijmst.2017.07.016>
- Niu WJ, Feng XT, Xiao YX, Feng GL, Yao ZB, Hu L (2021) Identification of potential high-stress hazards in deep-buried hard rock tunnel based on microseismic information: a case study. *Bull Eng Geol Environ* 80:1265–1285. <https://doi.org/10.1007/s10064-020-01973-x>
- Peng JY, Zhang FP, Yan GL, Qiu ZG, Dai XH (2019) Experimental study on rock-like materials fragmentation by electric explosion method under high stress condition. *Powder Technol* 356:750–758. <https://doi.org/10.1016/j.powtec.2019.09.001>
- Xiao SY, Su LJ, Jiang YJ, Liu ZX (2019) Numerical analysis of hard rock blasting unloading effects in high in situ stress fields. *Bull Eng Geol Environ* 78:867–875. <https://doi.org/10.1007/s10064-017-1067-7>
- Xu H, Feng XT, Yang CX, Zhang XW, Zhou YY, Wang ZF (2019) Influence of initial stresses and unloading rates on the deformation and failure mechanism of Jinping marble under true triaxial compression. *Int J Rock Mech Min Sci* 117:90–104. <https://doi.org/10.1016/j.ijrmms.2019.03.013>
- Yang LY, Ding CX (2018) Fracture mechanism due to blast-imposed loading under high static stress conditions. *Int J Rock Mech Min Sci* 107:150–158. <https://doi.org/10.1016/j.ijrmms.2018.04.039>
- Yang RS, Ding CX, Li YL, Yang LY, Zhao Y (2019) Crack propagation behavior in slit charge blasting under high static stress conditions. *Int J Rock Mech Min Sci* 119:117–123. <https://doi.org/10.1016/j.ijrmms.2019.05.002>
- Yao W, Xia KW, Jha AK (2019) Experimental study of dynamic bending failure of Laurentian granite: loading rate and pre-load effects. *Can Geotech J* 56:228–235. <https://doi.org/10.1139/cgj-2017-0707>
- Yi CP, Johansson D, Greberg J (2018) Effects of in-situ stresses on the fracturing of rock by blasting. *Comput Geotech* 104:321–330. <https://doi.org/10.1016/j.compgeo.2017.12.004>
- Yilmaz O, Unlu T (2013) Three dimensional numerical rock damage analysis under blasting load. *Tunn Undergr Sp Tech* 38:266–278. <https://doi.org/10.1016/j.tust.2013.07.007>
- Zhang FP, Peng JY, Qiu ZG, Chen QK, Li YH, Liu JP (2017) Rock-like brittle material fragmentation under coupled static stress and spherical charge explosion. *Eng Geol* 220:266–273. <https://doi.org/10.1016/j.enggeo.2017.02.016>
- Zhang FP, Yan GL, Peng JY, Qiu ZG, Dai XH (2020a) Experimental study on crack formation in sandstone during crater blasting under high geological stress. *Bull Eng Geol Environ* 79:1323–1332. <https://doi.org/10.1007/s10064-019-01665-1>
- Zhang W, Feng XT, Xiao YX, Feng GL, Yao ZB, Hu L, Niu WJ (2020b) A rockburst intensity criterion based on the Geological Strength Index, experiences learned from a deep tunnel. *Bull Eng Geol Environ* 79:3585–3603. <https://doi.org/10.1007/s10064-020-01774-2>
- Zhang XL, Yi HB, Ma HH, Shen ZW, Dragomirescu E (2018) Blast parameter optimization study based on a blast crater experiment. *Shock Vib* 2018:8031735. <https://doi.org/10.1155/2018/8031735>
- Zhao J, Feng XT, Zhang XW, Zhang Y, Zhou YY, Yang CX (2018) Brittle-ductile transition and failure mechanism of Jinping marble under true triaxial compression. *Eng Geol* 232:160–170. <https://doi.org/10.1016/j.enggeo.2017.11.008>